Proceedings of the XVII ECSMGE-2019
Geotechnical Engineering foundation of the future
ISBN 978-9935-9436-1-3

doi: 10.32075/17ECSMGE-2019-1109

XVII European Conference
ECSMGE 2019
Reykjavik
on Soil Mechanics
and Geotechnical Engineering

Geotechnical Challenges in Iceland

Challages de geotechnices d'Islande

S. Erlingsson
Faculty of Civil and Environmental Engineering, University of Iceland, Reykjavik, Iceland
VTI – The Swedish National Road and Transport Research Institute, Sweden.

ABSTRACT: The geotechnical challenges in Iceland are in many aspects unusual. The geological setting of the country is unique and has a great influence on the local geotechnical conditions. Iceland lies on the divergent boundary between the Eurasian plate and the North American plate formed by the Mid-Atlantic Ridge. This has created a landmass with active volcanoes, geothermal areas and zones of high seismicity. The bedrock is relatively young and mainly basaltic. It has been built up of relatively thin lava layers during eruptions. It is frequently highly jointed with irregular interlayers. The horizontal stresses in the rock mass are furthermore very low. The soil layers consist mainly of non-cohesive materials, often created in catastrophic events such as glacial floods, and are therefore often loosely packed. This paper gives a short overview of the geotechnical conditions in the country and additionally describes several geotechnical engineering projects. Some geotechnical challenges due to climate change will also be briefly discussed.

RÉSUMÉ: Les défis géotechniques en Islande sont à bien des égards inhabituels. Le cadre géologique du pays est unique et a une grande influence sur les conditions géotechniques locales. L'Islande se trouve sur la frontière divergente entre la plaque eurasienne et la plaque nord-américaine formée par la dorsale médio-atlantique. Cela a créé une masse continentale avec des volcans actifs, des zones géothermiques et des zones de haute sismicité. Le substratum rocheux est relativement jeune et principalement basaltique. Il a été construit de couches de lave relativement minces pendant les éruptions. Il est souvent très joint avec des intercouches irrégulières. Les contraintes horizontales dans la masse rocheuse sont en outre très faibles. Les couches du sol sont principalement constituées de matériaux non cohésifs, souvent créés lors d'événements catastrophiques tels que les inondations glaciaires, et sont donc souvent emballés. Cet article donne un bref aperçu des conditions géotechniques dans le pays et décrit en outre plusieurs projets d'ingénierie géotechnique. Certains défis géotechniques dus au changement climatique seront également brièvement.

Keywords: Geotechnical engineering, geology, Iceland, rock mass, soils, material properties.

1 INTRODUCTION

Geotechnical engineering is a relatively young discipline in Iceland. Until the last decade of the nineteenth century the country was poor and isolated. Construction activities had been only minor and had not required any civil engineering knowledge. The first bridges for river crossings were made in the southern part of the country in

the 1890's. In the early twentieth century, the government started to investigate the possibilities of building a harbour in the capital area. The main pressure came from the traders and merchants who needed better and more secure quays for their loading and unloading their ships (Friðriksson 2013). In 1913 the construction of the Reykjavík harbour finally started. Four years later the first three piers that made up what is now called the Old Harbour had been erected. The earth and rock materials needed for the construction were transported about 3 km on specially built rail lines from quarries in nearby Öskjuhlíð and Skólavörðuholt. The harbour was the country entry to modern times for more secure export of fish products, improved trading and efficient transportation (Friðriksson 2013).

The next large engineering project was the construction of irrigation canals in the South Iceland lowland area between 1923 and 1930 to mitigate and control the discharge over agricultural land. It was at that time an engineering achievement requiring precise surveying followed by hydrological and hydraulic design based on a thorough understanding of fundamental geotechnical conditions. It was a successful project and benefitted farming in the area for many decades (Þórðarson 2002).

The beginning of exploitation of domestic energy resources started in 1920's, first and foremost to generate electricity from hydropower. The first power plant of any importance was the Elliðarárstöð, inaugurated in 1921, after only two years of construction time, providing almost one MW of electricity to the fast-growing city of Reykjavik (Þórðarson 2002). The location of the Elliðarár station was in the outskirts of the Reykjavík area, requiring only short transmission lines. The next phase in harnessing hydropower in Iceland was the construction of three hydropower stations by the River Sog, built in 1935 – 1960 about 50 km east of Reykjavík (Bjarnason et al. 2019). The third phase of hydropower utilisation began in the late 1960's on the River Þjórsá in South Iceland with several relatively big dams and associated reservoirs culminating with the Kárahnjúkar hydropower plant (690 MW) in East Iceland completed in 2009 (Bjarnason et al. 2019). Another pioneering engineering project during the last century was the utilisation of the geothermal energy which today is used to heat over 90% of houses in Iceland and produces about 27% of the electricity (Flóvenz 2019). This of course required good geotechnical skills as well as accountable and responsible construction practices. About 85% of the total primary energy supply in the country comes from domestically produced renewable energy sources. This is the highest share of renewable energy in any national total energy budget (Bjarnason et al. 2019).

The modern roads and bridge building era started in 1891 when the first suspension bridge over the River Ölfusá was erected. The bridge collapsed in 1944 due to overloading from two trucks transporting dairy products to the capital area (Þórðarson 2002). Gravel roads were thereafter gradually extended out from the capital area. In the 1960's construction was started of more permanent pavements with concrete or asphaltic surfaces. In 1974 the Icelandic ring road was completed. The construction of the last section of the ring road was a considerable challenge to geotechnical and hydraulic engineering due to the proximity to the Vatnajökull glacier and huge glacial floods.

The objective of this paper is to give a brief overview of the geotechnical and rock mechanical conditions in Iceland. As they are highly influenced by geological and geophysical processes, these are addressed as well. Examples of some typical challenges are given.

Finally, new challenges that we are facing within the field, such as climate change, will be discussed.

2 GEOLOGICAL SETTINGS

The geological setting of Iceland is unique. Iceland lies on the divergent boundary between

two tectonic plates, the Eurasian plate and the North American plate located squarely on the Mid-Atlantic Ridge (MAR) (Einarsson 2008, Thordarson and Höskuldsson 2014). Furthermore, the island is situated on a hotspot, the Iceland plume. The plume has probably, through its activity, caused the formation of the island with its first appearance over the ocean surface about 16 to 18 m years ago (Flóvenz 2019). The MAR enters the island from the south-west on the Reykjanes Peninsula and departs from the north-east coast. As the spreading axis crosses the island, it manifests a zone of active spreading and volcanism, the axial volcanic zones (AVZ) (Flóvenz 2019).

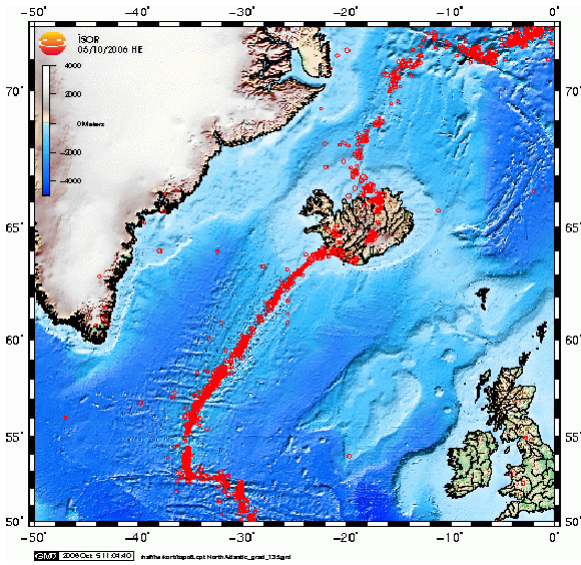

Figure 1. Epicentres of earthquakes in the Atlantic Ocean 1964–2006. Data are from the epicentre list of the NEIC, US Geological Survey. Figure courtesy of P. Einarsson.

As the AVZ passes through the country, it forms an irregular pattern. It has shifted about 150 km eastwards, close to the southern shoreline, forming the South Icelandic Seismic Zone (SISZ) and back north-west through the Tjörnes Fracture Zone (TFZ) on the northern cost. Between the two fracture zones (FZ), two parallel spreading segments are active but join into one segment north of the Iceland plume. There is active volcanism along the AVZ associated with this geological anomaly. Additionally there is earthquake activity, both along the ridges themselves and the two FZ (SISZ and TFZ) and geothermal fields along the rift zones as well as on both its flanks.

Figure 1 shows the epicentres of earthquakes on the Mid-Atlantic Ridge during the period 1964 – 2006. It shows that the epicentres form a narrow deformation zone south and north of the country, but as it crosses the Iceland plateau the zone becomes wider. This can also be seen in Figure 2.

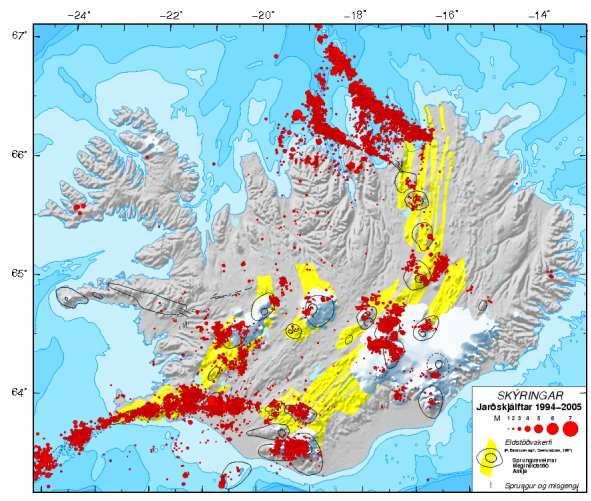

Figure 2. Earthquake epicentres, 1994 – 2007 and volcanic systems of Iceland. Epicentres are from the data bank of the Icelandic Meteorological Office. Figure courtesy of P. Einarsson.

A simplified geological map of Iceland is shown in Figure 3 where all the main geological subdivisions are indicated (Thordarson and Höskuldsson 2014).

.

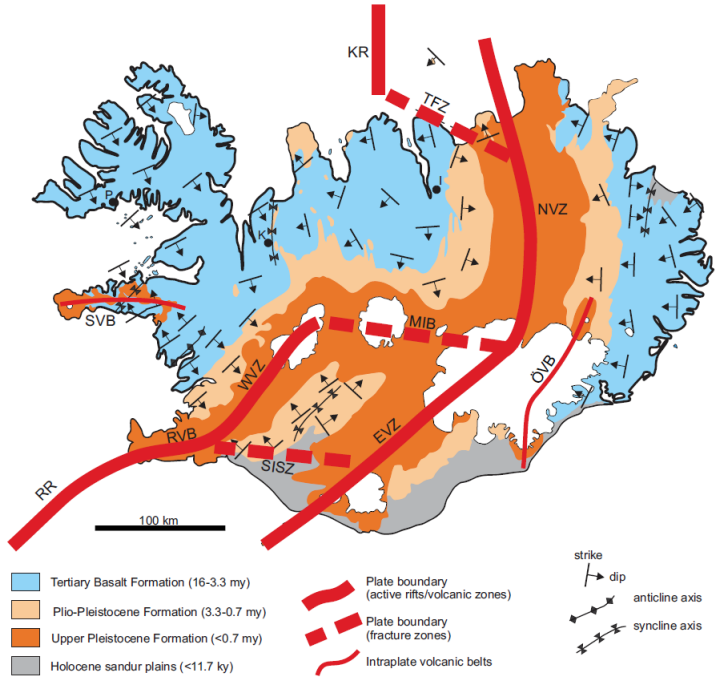

Figure 3. Simplified geological map of Iceland showing the main geological subdivisions as the fault structures, volcanic zones and belts. RR is the Reykjanes Ridge, RVB Reykjanes Volcanic Belt, WVZ West Volcanic Zone, MIB Mid-Iceland Belt, EVZ East Volcanic Zone, NVZ North Volcanic Zone, SISZ South Iceland Seismic zone, TFZ Tjörnes Fracture Zone, KR Kolbinsey Ridge, ÖVB Öræfi Volcanic Belt, SVB Snæfellsnes Volcanic Belt. Figure courtesy of Á. Höskuldsson.

The AVZ follows the divergent plate boundary where hot magma wells up vertically from the mantle and the two plates diverge horizontally. The new material then fills in the gap between the plates, thus increasing the overall size of the main island. This lateral movement can be observed on the surface (Árnadóttir et al. 2009). Figure 4 shows the observed lateral movements of the surface measured during the period 2004 – 2016 with the GPS technique (Valsson 2019). On average, this gives a movement of 19 mm/year (stations close to the SISZ earthquake in 2008 and to the volcanic eruption in Holuhraun in 2014 ignored).

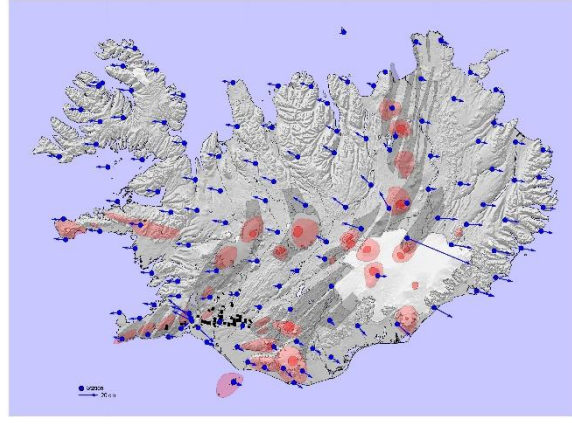

Figure 4. Observed lateral displacement measured with the GPS technique in Iceland during 2004 to 2016. Figure courtesy of G. Valsson.

Figure 5 shows a simplified overview of the geothermal fields of Iceland. The high temperature areas follow the AVZ. On both flanks of the AVZ, an irregular band of low temperature areas is formed. However, at a considerable number of locations low temperature fields have been observed further away from the AVZ.

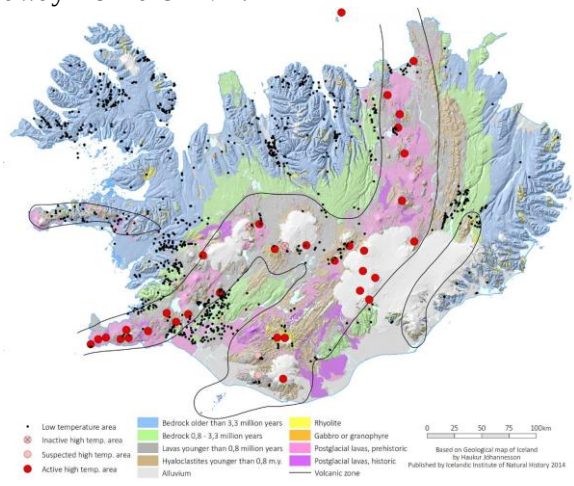

Figure 5. Geothermal fields in Iceland. Figure courtesy of H. Bjarnason.

Figure 6 shows typical temperature logs in boreholes in Iceland outside the AVZ (high temperature geothermal areas) (Flóvenz 2019). The figure shows that the temperature in the uppermost five hundred metres can vary from very low temperatures to almost 80°C. Thus, from a geotechnical point of view, at very many locations the risk of encountering high temperatures in the ground needs to be considered.

3 ROCK ENGINEERING

The geological and geophysical settings have a major impact on the local rock engineering characteristics and therefore their applications in engineering such as foundations, dam and bridge abutments, stability of underground openings and aggregate productions.

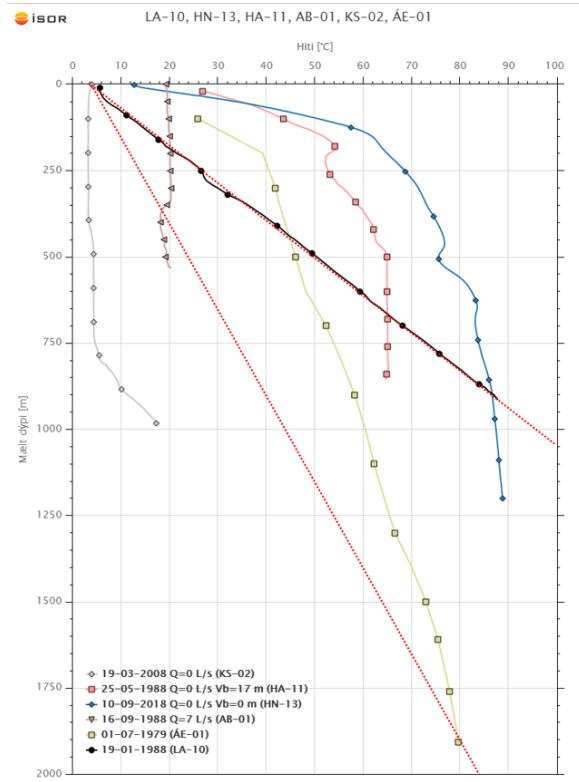

Figure 6. Temperature logs in a few boreholes in Iceland. Figure courtesy of Ó. Flóvenz.

As stated before, Iceland is a volcanic island created by volcanism on the MAR during the last approximately 18 million years. Most of the rock formations in Iceland are therefore of volcanic origin from the late Tertiary to the present time. The oldest rock is in the extreme east and west of Iceland where the rock mass is in general built up of sub-horizontal strata of regional basalt layers, most often with scoriaceous interfaces between the adjacent basaltic layers and sedimentary interbeds (Loftsson et al. 2005). Inclined dikes or other discontinuities appear frequently. The basaltic lava can be highly fractured. Figure 7 gives a schematic overview of a melted lava stream running over existing land. The lava cools off from the surface and the bottom, creating highly fractured zones. With time the inner part cools off as well, creating shrinkage joints in the rock mass.

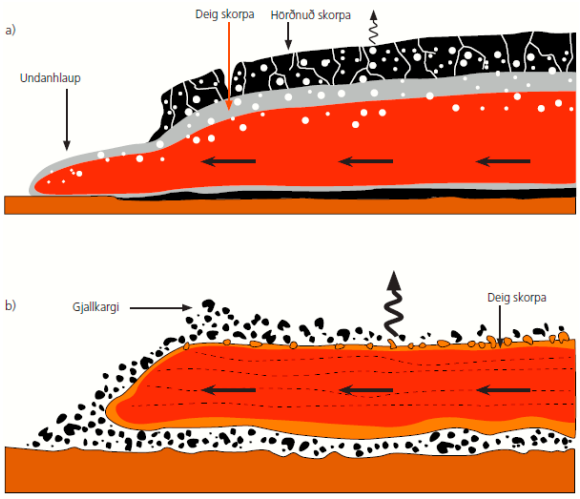

Figure 7. Melted lava flowing over existing land. The moving lava cools off from the surface and the bottom, creating highly fractured zones. Sólnes et al. 2013 (Þ. Þórðarson).

Figure 8 shows a typical Icelandic lava stratum.

Figure 8. Cross section of typical Icelandic rock mass. Horizontal lines can be seen, forming boundaries between different lava layers. The layers are usually a few to tenths of metres in thickness.

3.1 Mechanical properties

The main engineering properties of intact rock samples are strength and deformation. An example of a measurement of the stiffness and Poisson's ratio from a uniaxial compression test of basalt and scoria is given in Figure 9 (Jóhannsson 1997). The samples were from the Hvalfjörður tunnel that was completed in 1998.

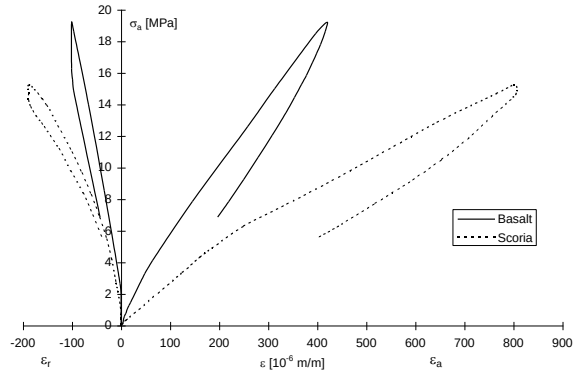

Figure 9. Stress-strain relationship of basalt and scoria in one-dimensional compression test. The indices a and r refer to the axial and radial directions, respectively.

3.2 In situ rock mass stress

Measurements of rock stresses have been made in combination with various underground projects throughout the country during the last 50 years with the hydraulic fracturing and overcoring methods (Loftsson et al. 2006, Hemmingsen 2016). The vertical stress components can be assumed to follow the worldwide trend with an increasing slope of 0.027 MN/m^3 with depth. The horizontal stresses, on the other hand, are unconventional. The horizontal stresses are usually expressed as the rock stress coefficient *k* defined as

$$k = \frac{\frac{1}{2}(\sigma_h + \sigma_H)}{\sigma_v} \quad (1)$$

where σ_h, σ_H and σ_v are the minor and major horizontal and vertical stress components, respectively. The results of the rock stress coefficient measurements as a function of depth are shown in Figure10.

Table 1. Some typical technical properties of common Icelandic bedrock (based on Guðmundsson et al. 1991).

Porperty	*Basalt*	*Scoria*	*Sedim. rock Fine-grained*	*Sedim. rock Coarse-grained*	*Fault Breccia*
UCS [MPa]	100 – 300	20 – 60	5 – 30	5 – 80	1 - 20
E [GPa]	20 – 60	2 – 20	2 – 10	2 – 15	?
Q – value [-]	4 -12	3 – 10	0.1 – 3	0.5 – 4	0.01 1.0
Typical strata thickness [m]	2 – 15	0.5 – 5	0.2 – 5.0	1 – 10	0.1 – 2

UCS is the Uniaxial Compression Strength of intact rock specimens of 50 mm in diameter.
E is the Young modulus (stiffness) of intact rock specimens.
Q-value is the NGI Quality value (https://www.ngi.no/eng/Services/Technical-expertise-A-Z/Engineering-geology-and-rock-mechanics/Q-system)

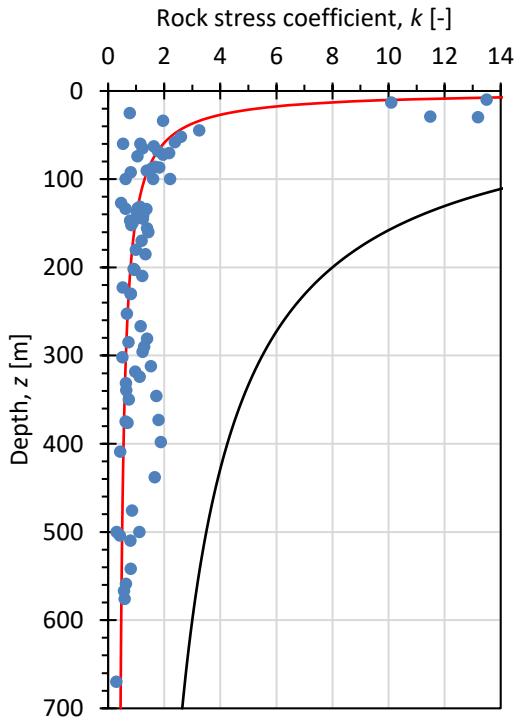

Figure 10. Rock stress coefficient as a function of depth from 17 stress measurement locations in Iceland. The black and red lines represent the upper and lower boundaries based on worldwide trends.

The red and black lines represent the worldwide lower and upper limit trends (Hudson and Harrison 2002) expressed as

$$\frac{100}{z}+0.3<k<\frac{1500}{z}+0.5 \qquad (2)$$

where z is in metres.

As can be seen in Figure 10 the rock stress coefficient is generally very low and many measurements reveal values that are even lower than the lower boundary trend implicates. The reason for these low horizontal stresses is probably due to the divergent plate movements at the MAR which generate a pulling force in the crust that reduces horizontal compression.

A simple relationship between the k-value and the horizontal deformation modulus E_h exist as

$$k=0.25+7E_h\left(0.001+\frac{1}{z}\right) \qquad (3)$$

where E_h is given in GPa and z in m (Sheory 1994). The previously obtained results are shown in Figure 11 along with three E_h values.

Based on Figure 11 it is clear that the deformation moduli in the country lie mainly between 4 and 35 GPa, particularly at depths shallower than 300 m. At one location in the oldest bedrock (furthest away from the rift zone) a deformation modulus as high as 70 GPa was observed at depths greater than 300 meters.

3.3 Underground openings

There are basically two types of underground openings constructed in the country, i.e. as a part of hydropower schemes (access, headrace- & tailrace tunnels, vertical shafts, power houses) and road tunnels. The building of underground openings began in 1948 with the 30m long Arnardalshamar road tunnel and culminated in 2004 – 2008 with the construction of the Kárahnjúkar hydropower plant where all together 73 km of tunnels were built, of which around 48

km were full face TBM bored tunnels (Loftsson et al. 2005; Bjarnason et al. 2019).

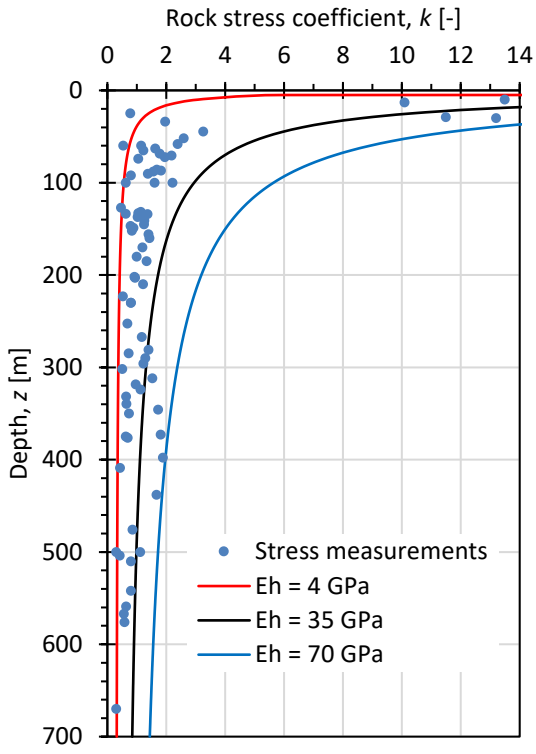

Figure 11. Rock stress coefficient as a function of depth. The lines represent three values of the horizontal deformation modulus.

The structural stability design of the underground openings has almost solely been based on the *Q*-system (NGI 2015). The reinforcement strategy presented there works well over the entire range of *Q*-values. i.e. from spot bolting in extremely good conditions through systematic bolting and fibre reinforced shotcrete to rib reinforcements in very or extremely poor conditions.

The main problems that occur in rock mass underground openings are usually related to:

Water leakage
Geothermal heat
Layered strata
Sedimentary layers

The rock mass is often highly fractured, with thin layers and irregularly directed dikes and other weakness planes. Furthermore, the horizontal stresses are low. The permeability of the rock mass can therefore be expected to be high. In areas with high groundwater table a large inflow of water has occurred that has been difficult to control.

In areas where the heat gradient is high, the rock mass can in some areas have a temperature up to 70 – 80 °C at depths of just a few hundred metres. Where water inflow has also taken place, this has caused difficult working conditions.

The fact that the strata are built up of thin layers ranging from a few tens of cm to a few metres or tens of metres that frequently further dip from horizontal, means that tunnels are always crossing new layer interfaces. The rock face consists therefore frequently of mixed layers of materials with different mechanical properties. Stress concentrations can therefore be observed at the layers´ boundaries, and if a weak layer appears in the crown the risk of instability is high.

4 SOIL CONDITIONS

The local soil conditions consist mostly of normally consolidated Holocene soils of basaltic origin. The soils have been created by glacial or weather erosion and transported by aerial or fluvial processes, usually from the central plateau towards the coast. Some soil movement occurred in catastrophic events, such as in volcanic eruptions or by glacial floods. This means mostly that the local soils are coarse-grained aggregates (coarse silty particles and coarser grains) that are often loosely compacted. The finer fractions, which settle in low streams, are transported to the sea. An example of typical soil conditions is shown in Figure 12 where a newly constructed bridge over the River Morsá is shown in the foreground and the Öræfajökull Glacier (part of the Vatnajökull) in the background. The soils shown are fluvial sandy or gravelly soils and have been transported mainly in catastrophic events originated from volcanic or geothermal activity under the Vatnajökull Glacier.

Figure 12. Thick sediments of loosely compacted sandy and gravelly soils in the forefront that have been piled up mainly in catastrophic events such as volcanic eruptions or glacial flow. Figure courtesy of by V. A. Ingólfsson.

Figure 13. Mt. Hekla has created thick sediments of pumice in prehistoric eruptions. Sólnes et al. 2013 (Pálmi Hannesson/Sólarfilma).

Additionally there are soils that have been created in volcanic eruptions. Ash and pumice from Holocene volcanic eruptions can be found in some areas such as near some of the active volcanoes. Pumice is a lightweight and highly porous material of low strength. However, it also has good thermal properties and has been used in mortar or as thermal isolation layers in construction (see Figure 13).

As in many northern European countries and in North America peat deposits can be found in some places in Iceland. The local climate, geography and environment favour bog and peat bog formations. The peat is usually lightly decomposed with a high void content and water content as high as a few hundred to one thousand per cent. Figure 14 shows a thin road structure resting on peaty land. The pavement structure was damaged in the June 17, 2000, earthquake (M_w 6.5) due to liquefaction of the underlaying soft peat.

Figure 14. A pavement structure resting on a peaty subgrade in Holt, South Iceland that liquefied in the June 17, 2000 earthquake (M_w 6.5). Figure courtesy of V. A. Ingólfsson.

The main soil categories according to the Unified Soil Classification System (USCS) are gravel (G), sand (S) and silt (M) or mixtures of these fractions, as well as organic soils (peat). The fine particles (diameter < 63 μm) consist mostly of silt size fractions (between 2 and 63

μm); thus hardly any clayey soils can be found in the country.

4.1 Deformation properties

The deformation characteristics of the soils, for settlement predictions, are usually estimated with Janbu's Modulus Method (Janbu 1970). The load-deformation relationship is therefore estimated by a one-dimensional compressional (oedometer) test where the slope of the curve in the stress strain plot, the tangent modulus M_t, can be expressed as:

$$M_t = \frac{d\sigma'}{d\varepsilon} \tag{4}$$

where $d\sigma'$ and $d\varepsilon$ are the increments of effective stress and strain, respectively. The tangent modulus can be assumed to follow the relationship:

$$M_t = m\sigma_a \left(\frac{\sigma'}{\sigma_a} \right)^{1-a} \tag{5}$$

where m and a are material parameters and σ_a is a reference stress (100 kPa). By rewriting equation (4) and integrating, the strain can be estimated by

$$\varepsilon = \int_{\sigma'_0}^{\sigma'_0+\Delta\sigma'} \frac{1}{M_t} d\sigma' \tag{6}$$

giving

$$\varepsilon = \frac{1}{ma} \left[\left(\frac{\sigma'_0 + \Delta\sigma'}{\sigma_a} \right)^a - \left(\frac{\sigma'_0}{\sigma_a} \right)^a \right] \text{ if } a \neq 0 \tag{7}$$

or

$$\varepsilon = \frac{1}{m} \ln \left(\frac{\sigma'_0 + \Delta\sigma'}{\sigma'_0} \right) \quad \text{if } a = 0 \tag{8}$$

Based on a large amount of testing (Skúlason 1978) the two parameters, the modulus number m and the stress exponent a for saturated samples, have been estimated for different soil types (see Figures 15 – 17). The stress exponent can be assumed as 1.0 for coarse gravel, 0.5 for silt and sandy materials, and 0.0 for clay and organic (peaty) soils.

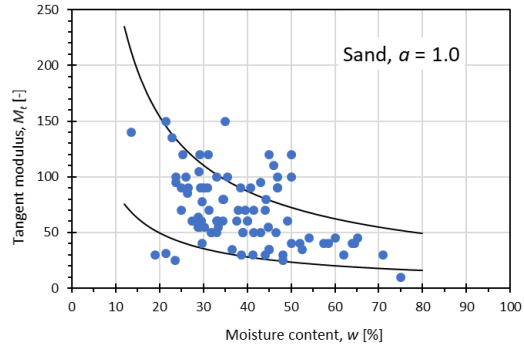

Figure 15. Tanget modulus M_t ($M_t = m\sigma_a$ as $a = 1.0$) of saturated sandy materials as a function of moisture content.

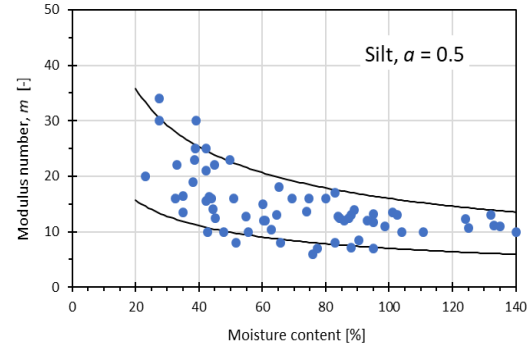

Figure 16. Modulus number m of saturated silty materials as a function of moisture content.

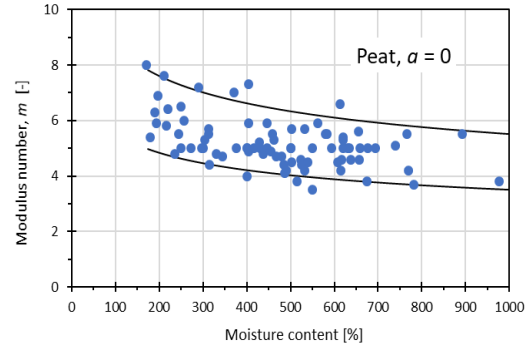

Figure 17. Modulus number m of saturated peat as a function of moisture content. Note that the moisture content is high, ranging from 150 – 1000%.

Furthermore, the soil types exhibit time dependent deformations that are not stress

dependent. Again, the soil parameter, the time resistance R, is usually estimated according to Janbus method (Janbu 1970), i.e.

$$R = \frac{dt}{d\varepsilon} = r_s\left(t - t_r\right) \quad t > t_r \tag{9}$$

where r_s is the time resistance coefficient and t_r is a reference time (for most soils it can be assumed that $t_r = 0$) (Skúlason 1978). The induced strain as a function of time can now be estimated as

$$\varepsilon_s = \frac{1}{r_s}\ln\left(\frac{t}{t_p}\right) \tag{10}$$

where t_p is the time for the primary consolidation.

The time resistance coefficient r_s for the three soil groups of sand, silt and peat are shown in Figures 18 – 20.

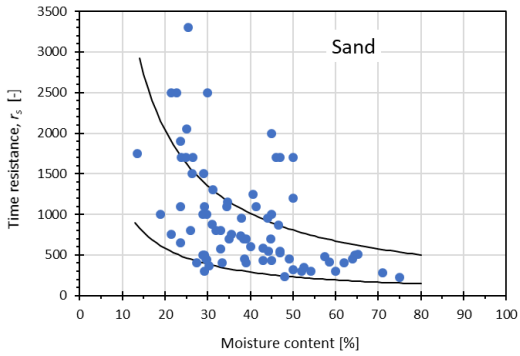

Figure 18. Time resistance coefficient r_s for sand as a function of moisture content.

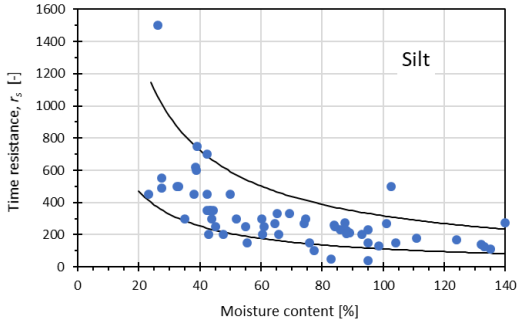

Figure 19. Time resistance coefficient r_s for silt as a function of moisture content.

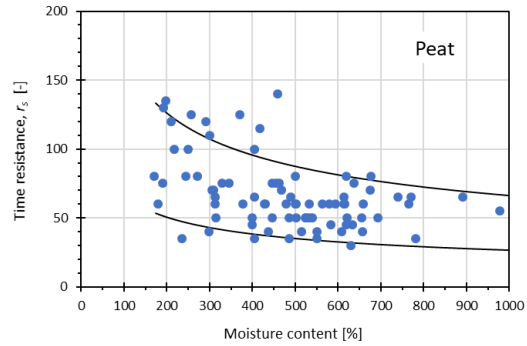

Figure 20. Time resistance coefficient r_s for peat as a function of moisture content. Note the high in-situ moisture content.

4.2 Strength characteristics

Most soils in Iceland are coarse-grained with a low fine content. Hence they are non-cohesive with no or little plasticity. The main strength parameter is therefore consequently the friction angle ϕ' and the cohesion c can be ignored. The friction angle in a compacted state is, however, relatively high as compared to many other regions. The reason for this is probably linked to the surface characteristics of the grains that are frequently angular with fresh surfaces and sharp corners that show good interlocking effects in a compacted state.

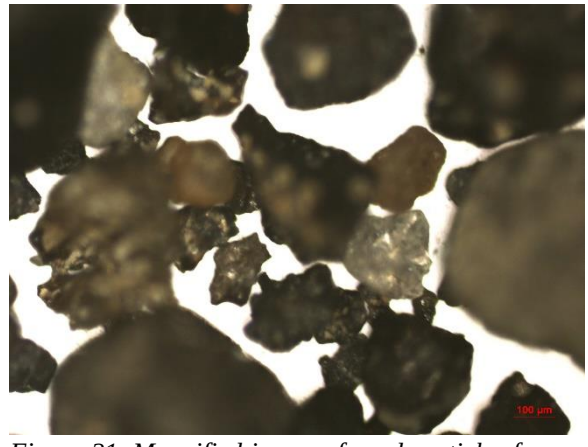

Figure 21. Magnified image of sand particles from a sample from test pit at the proposed Urridafoss HE project site (Wells 2009).

Common values of friction angles of well compacted materials are given in Table 2 (Skúlason et al. 2002, Pálmason 2018).

Table 2. Common friction angles for well compacted soils in Iceland.

Soil type	Friction angle [°]
Gravelly soil	50 – 65
Sandy soil	42 – 48
Silty moraine	40 – 47

4.3 Classification of soils

For soil exploration, dynamic sounding and rotary/percussion sounding have frequently been used successfully. They both suit well for coarse-grained materials and as the cone head or crown is robust, there is little risk of damaging during testing. In both methods, the rod can both be pushed downwards and rotated and can therefore penetrate through all soil types, ranging from fine-grained to very coarse- grained soils or rock. The interpretation of the data for soil classification is however somewhat difficult, although depth to firm ground (bedrock) can be estimated.

A Standard Penetration test (SPT) or Cone Penetration test (CPT) is further used. An example of CPT test results on the south coast at a location close to Þorlákshöfn is given in Figure 22. This is a site consisting of typical non-cohesive material with particle sizes ranging from silty particles and larger. Although the site deposit is very thick, the test was terminated at 8.3 m depth due to high resistance and consequently risk of damage to the CPT cone. This was probably due to the fact that the cone hit larger boulders that fequently occur in the local soils.

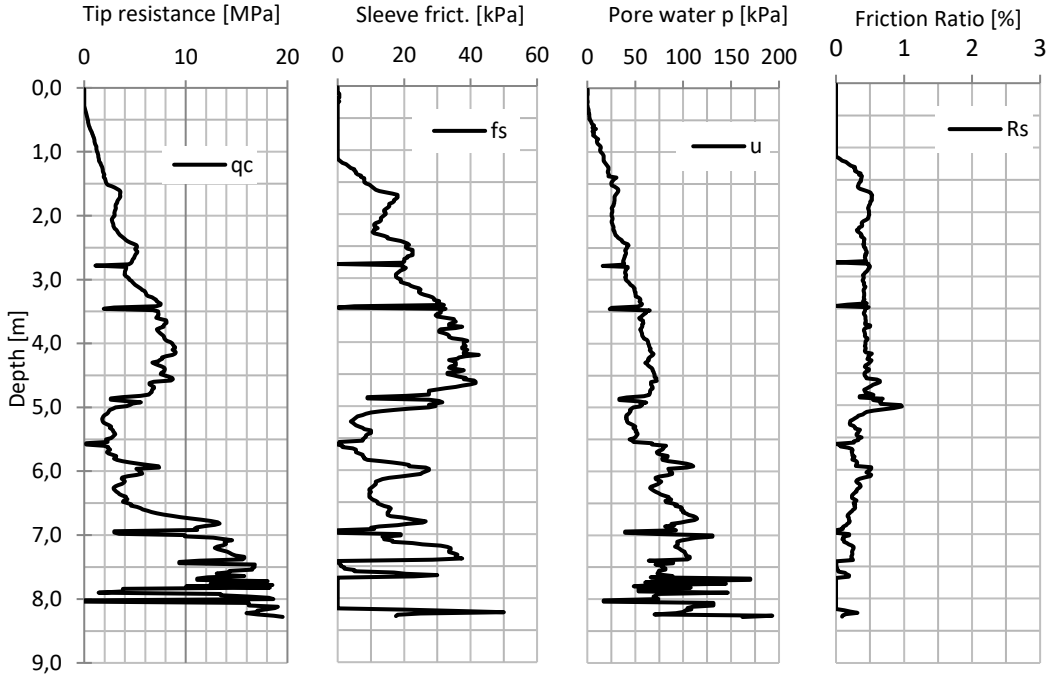

Figure 22. CPT results from a sandy site on the south coast close to Þorlákshöfn.

The results of the CPT measurements were then used to classify the deposit using the normalized soil behaviour type (SBTn) chart (Robertson 1990 and 2009) (see Figure 23). Most of the data points are classified as soil behaviour type 6 "sands – clean sand to silty sand". However, some data points, mainly in the depth range of 5.0-5.7 m, are classified as type 5 "sand mixtures – silty sand to sandy silt".

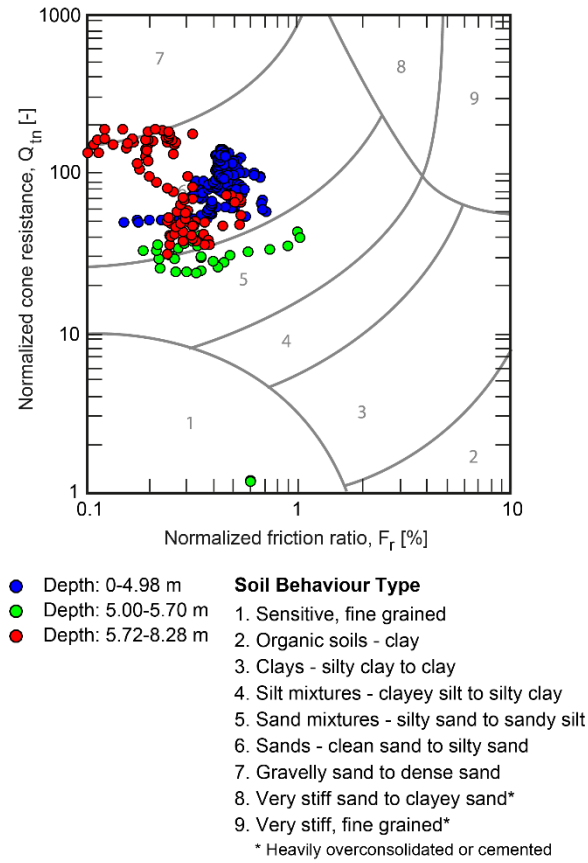

Figure 23. Normalized soil behaviour type (SBTn) chart with results of CPT measurements at the Þorlákshöfn site.

Multichannel Analysis of Surface Waves (MASW) measurements have subsequently been conducted at the site. The method is non-invasive and it is suitable on soft as well as coarse-grained soils. The method gives the shear wave velocity of the soil stratum (Park et al. 1999, Ólafsdóttir et al. 2018). Various correlation equations exist between shear wave velocity *Vs* and different CPT-related parameters, such as cone resistance (q_c), corrected cone resistance (q_t), sleeve friction (f_s), overburden stress (σ_{v0}), effective stress (σ'_{v0}) and depth (z). Examples of CPT-V_S correlations, either intended for sands or for all soil types, are provided in

Table 3 (Ólafsdóttir et al. 2019b, Erlingsson et al. 2017).

Table 3. Examples of CPT-V_S correlation equations.

$V_S \approx 17.48 q_c^{0.13} (\sigma'_{v0})^{0.27}$	Baldi et al. (1989)
$V_S \approx (10.1 \log(q_c) - 11.4)^{1.67} \left(\frac{100 f_s}{q_c}\right)^{0.3}$	Hegazy and Mayne (1995)
$V_S \approx 118.8 \log(f_s) + 18.5$	Mayne (2007)
$V_S \approx 32.3 q_c^{0.089} f_s^{0.121} z^{0.215}$	Piratheepan (2002)
$V_S \approx 134.1 + 0.0052 q_c$	Sykora and Stokoe (1983)

q_c, q_t, f_s, σ_{v0} and σ'_{v0} in kPa and z in meters. $p_a = 100$ kPa.

The CPT-V_S correlations in Table 3 were applied to the acquired CPT data. Figure 24 compares the V_S-profiles predicted based on the CPT-V_S correlation equations and the profile that was obtained by the MASW method.

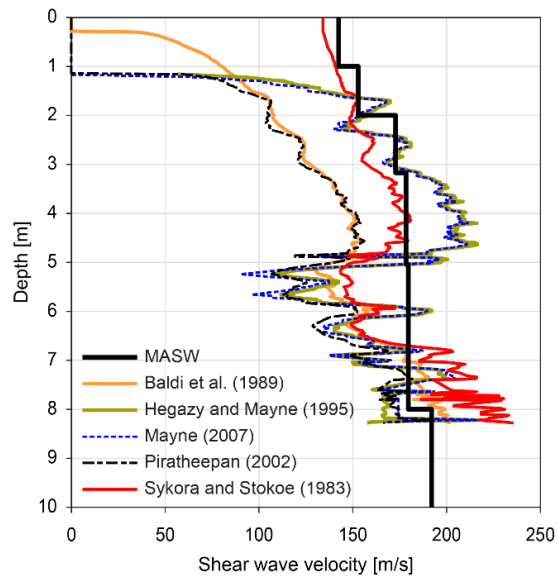

Figure 24. V_S-profiles for the Þorlákshöfn site predicted based on selected CPT-V_S correlations and obtained by MASW.

One can see in Figure 24 that the proposed equation by Sykora and Stokoe (1983) fits the data relatively nicely. It is necessary, however, to bear in mind that this is a relatively shallow profile. Further validation is needed.

5 INFRASTRUCTURE PROJECTS

Geotechnical engineering and engineering rock mechanics have played a major roll in forming modern Icleand, in building the road infrastructure, and harnessing of hydropower and geothermal energy, as well as in the construction of the ports and harbours along the coast.

Here are a few examples of projects to give the reader insight into problems that we have been facing.

5.1 Rock tunnels

As of today, 14 road tunnels are part of the road network for a total of over 65 km of tunnels. Most tunnels include two lanes, giving a cross-sectional area of around 55 m^2. In addition, the total length of tunnels associated with hydropower utility is around 85 km with a cross-section area that varies from 6 to over 150 m^2 (Loftsson et al. 2005) Reinforcement is mainly designed according to the Q-system and on average around 3 rockbolts (3 m long) are used per metre for tunnels with ~8 m span (cross section around 54 m^2) and 2.5 m^3/m of fibre-reinforced shotcrete. If conditions are very poor shotcrete ribs or lattice girders provide additional support that has been proven to be both economic and durable. An example of using lattice girders is shown in Figure 25.

Due to the Tertiary volcanic activity the local bedrock is piled up in thin layers, frequently with interlayers. An example of a tunnel face from the Vaðlaheiði road tunnel is shown in Figure 26. In the crown a basaltic layer can be seen with a thin layer of scoria underneath. Below this there is a soft red sedimentary layer resting on a thin scora/basalt layer on top of another thin brownish sedimentary layer. Finally, in the insert a new scoria and basalt layer can be seen.

Figure 25. Lattice girders as a support in the 2-lane Vaðlaheiði road tunnel. Figure courtesy of B. A. Harðarson.

Figure 26. Drilling into a layered face at the Óshlíð road tunnel. Figure courtesy of B. A. Harðarson.

The general low horizontal stresses and frequently fractured rock mass with irregular interbeds can lead to major water inflow into tunnels if excavation takes place under the groundwater table in the rock mass. This has happened in some tunnel excavations such as the Vestfjörður tunnel, Héðinsfjarðar tunnel and Vaðlaheiði tunnel, leading to delays and increased cost. An example of a water inflow into the Héðinsfjörður tunnel is shown in Figure 27.

Figure 27. Water inflow into the Héðinfjörður tunnel. Figure courtesy of B. A. Harðarson.

5.2 Hydropower utility and dams

Iceland's numerous rivers are relatively short but with a large head and high run-off. This makes them very suitable for generating electricity. As of today hydropower accounts for almost 73% of all electricity production in Iceland (Bjarnason et al. 2019). Harvested electricity comes mainly from glacial rivers that have a seasonally varied flow rate. Water reservoirs with associated dams are therefore necessary. Today 29 dams in Iceland meet the criteria set by ICOLD (International Commission on Large Dams) for large dams. The oldest one is the Skeiðfoss dam, a concrete buttress structure constructed in 1945, and the most recent one is the Sporðalda dam commissioned in 2013 (Bjarnason et al. 2019). Most dams are earth-rockfill dams with a central impervious moraine core (23 dams), abutted by gravel filters, supporting fills and riprap for erosion and wave protection. Other types of large dams in Iceland are two concrete-faced rock fill dams (CFRD), one asphalt concrete-faced dam, one gravity dam and two buttress dams. A cross section of Búrfell dam is given in Figure 28.

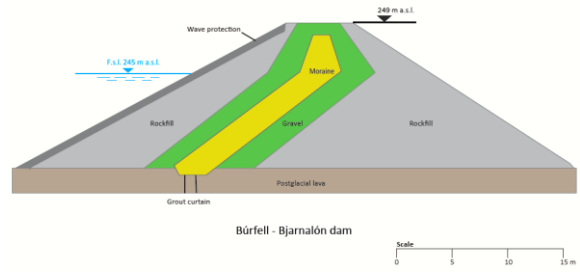

Figure 28. Cross section of the 5.9 km long and 33 m high Búrfell dam. The core consists of local loessic soil with alluvial gravel filter material and rock-fill shells. Figure courtesy of H. Bjarnason.

Many of the hydropower stations are located in the Þjórsá-Tungná-Kaldakvísl area in the outskirts of the SISZ. Seismic aspects need therefore to be taken into account in the design process. An attempt was made in 2018 to assess the shear stiffness of three dam structures (Ólafsdóttir et al. 2019a) using the MASW technique (see Figure 29). The purpose was to estimate their structural health and to create a base in order to be able to observe potential changes in the future.

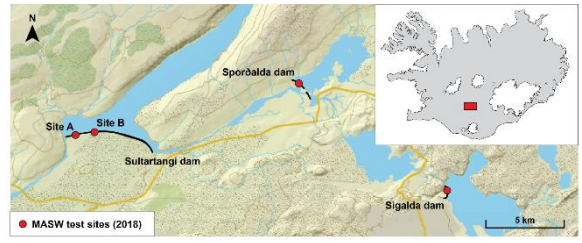

Figure 29. Location of MASW test sites at Sigalda dam, Sporðalda dam and Sultartangi dam. [The map is based on data from the National Land Survey of Iceland.].

Results from the two MASW measurments at the Sultartangi dam are shown in Figure 30.

.

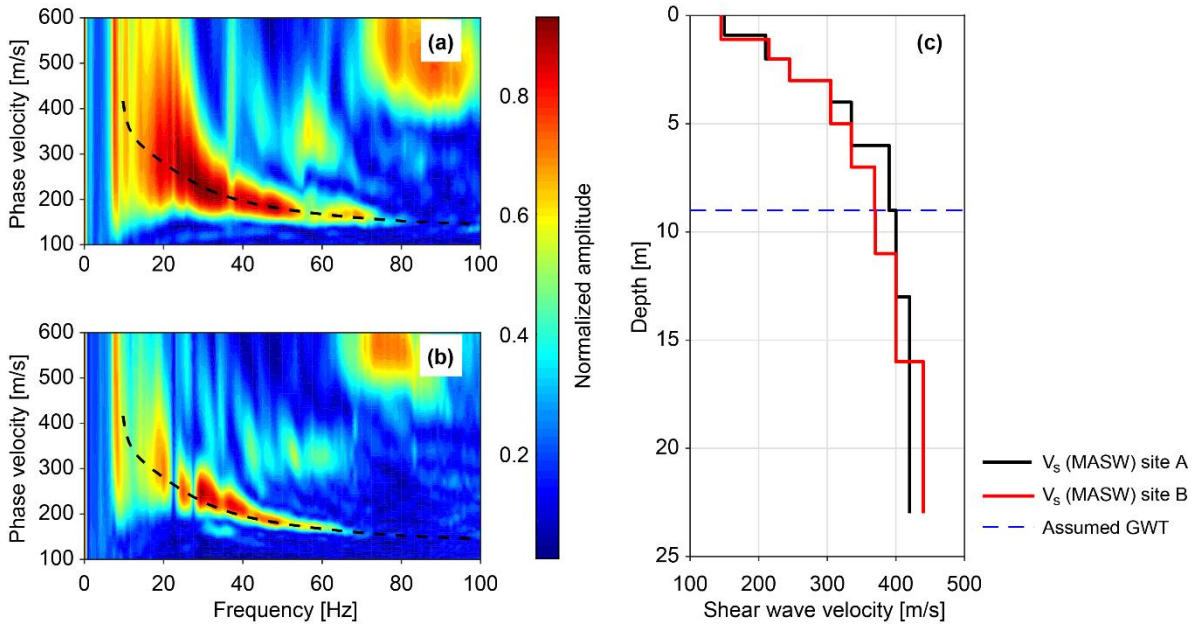

Figure 30. Results of MASW measurements at two locations on the crest of the Sultartangi dam (site A and B). Dispersion images obtained at Sultartangi site A by using survey profiles of length (a) 11.5 m and (b) 23 m. Estimated (c) shear wave velocity (V_S). The theoretical dispersion curve corresponding to the V_S-profile for site A is shown using a black dashed line in (a) and (b). The assumed location of the groundwater table (GWT) within the central core of the dam is shown using a blue dashed line in (c).

A simple model proposed by Seed and Idriss was therafter used to estimate the small-strain shear modulus of the dams

$$G_{\max} = 1000 K_{2,\max} \sqrt{\sigma'_m} \qquad (11)$$

where $K_{2,max}$ (kPa$^{0.5}$) is an empirical coefficient (Gazetas 1991, Kramer 1996).

The results are presented in Figure 31. They indicate that the experimentally evaluated small-strain shear stiffness profiles can in general be fitted adequately with the empirical model. A value of $K_{2,max}$ in the range of 30-35 seems to provide the best fit between the experimental and empirical stiffness profiles for the Sigalda and Sporðalda dams. However, for the two test sites on the crest of the Sultartangi dam (where the central core was primarily made of loess), a slightly lower value of $K_{2,max}$, or between 25-30, appears to provide the closest match. It can be further noted that a $K_{2,max}$ in the range 25 – 40 is classified as very dense sand and gravel (Gazetas 1991).

.

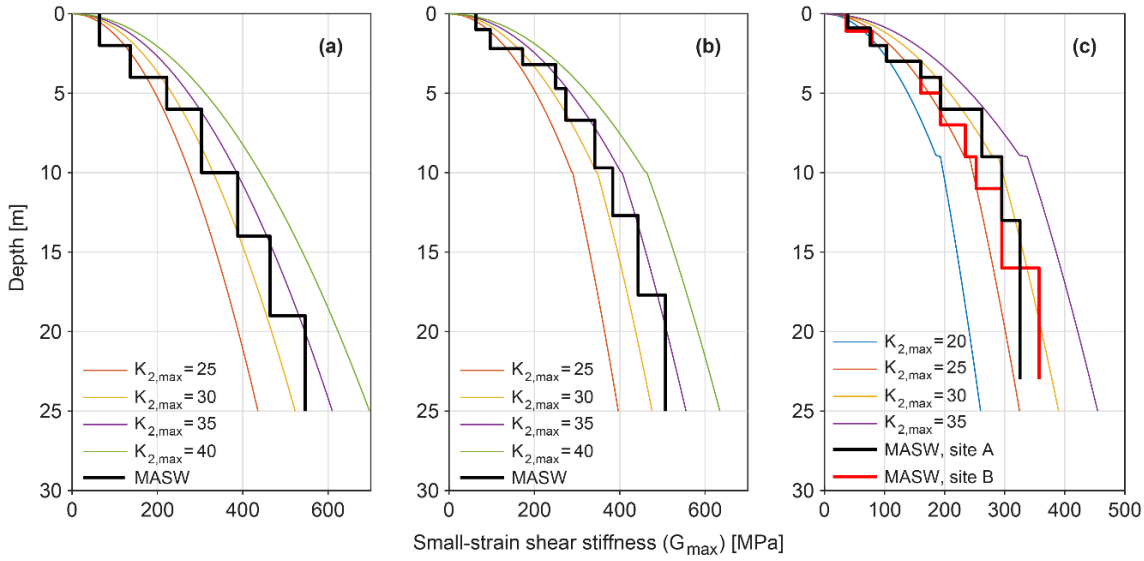

Figure 31. Comparison of empirical and experimental stiffness profiles for the (a) Sigalda dam site, (b) Sporðalda dam site and (c) Sultartangi dam sites. The empirical profiles were obtained by the model of Seed and Idriss using four different $K_{2,max}$ values.

In 2009 the Kárahnjúkar hydropower project (690 MW) was completed. It included the creation of the Hálslón reservoir (2100 Gl) by construction of three dams: two earth-rock-fill dams, the Desjará Dam and the Sauðárdalur Dam, and the concrete-faced rock fill (CFRD) Kárahnjúkar Dam that is the highest CFRD of its kind in Europe, 198 m (Bjarnason et al. 2019).

Kárahnjúkar Dam, the Desjará Dam and the Sauðárdalur Dam are shown in Figure 32.

5.3 Sesimic Hazard

In 2000 two earthquakes occurred within the SISZ with only a 4 day interval, on the 17th and 21st of June. Their magnitudes were both M_w6.5. Eight years later on May 29, 2008, the third earthquake hit the area (M_w6.3). Considerable damage was observed but no casualties (Einarsson 2008, Sigbjörnsson et al. 2009). Liquefaction was observed at Arnarbæli in the western part of the SISZ where sand boils were found on the bank of the River Ölfusá (Fig. 33).

Figure 32. Hálslón Reservoir area; the Desjará Dam to the left, the Kárahnúkar Dam and spillway in the middle, the Sauðárdalsstífla Dam to the right. The Brúarjökull Glacier (part of the Vatnajökull Glacier) in the background. Figure courtesy of H. Bjarnason.

The Arnarbæli site is located less than 1 km from the active fault that ruptured in the 2008 earthquake. The estimated peak ground acceleration (PGA) for the site a_{max} was in the range of 0.6–0.7g. The soil at the Arnarbæli site consists of loosely compacted glaciofluvial volcanic sand. The soil stratum is uniform down

to a great depth with the groundwater table close to the surface. Soil samples were collected at the Arnarbæli site by Green et al. (2012). The fine content of the material is around 7% and its grain size distribution lies well within the boundaries for potentially liquefiable soils, and partially within the boundaries identified as "most liquefiable soils" (Green et al. 2012; Tsuchida 1970).

Figure 33. Sand boils (liquefaction) on the bank of the River Ölfus close to the epicentre of the 29 May 2008 M_w6.3 earthquake. Figure courtesy of O. Sigurðsson.

A liquefaction resistance curve (V_{S1} – CRR curve) scaled to account for the effects of an M_w6.3 earthquake is presented in Fig. 34. The cyclic stress ratio and the normalized shear wave velocity were calculated for reference points at a depth ranging from 0.3 – 20.7 m and compared to the liquefaction resistance curve. The PGA of the site was estimated as 0.65g. The results presented in the figure indicate that liquefaction had occurred at the site down to around a 4 m depth.

The complex local lava bedrock piles additionally show some unexpected behaviour. One such example is reported in Bessason and Kanyia (2002). In the June 17, 2000, earthquake (M_w 6.5) strong ground motion was recorded at both abutment piers of the 83 m long Thjórsá bridge, which is located in the SISZ. The east pier of the bridge is resting on bedrock but the west pier is resting on a 9 m thick Tertiary laval layer resting on a 20 m alluvial sand deposit on top of the bedrock (Figure 35).

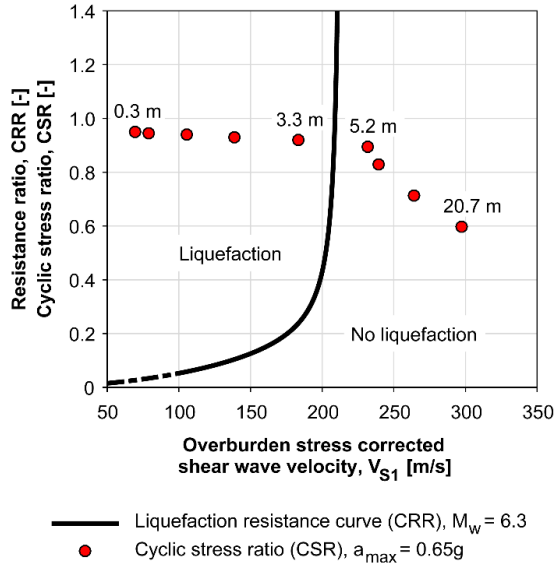

Figure 34. Liquefaction evaluation chart for the Arnarbæli site.

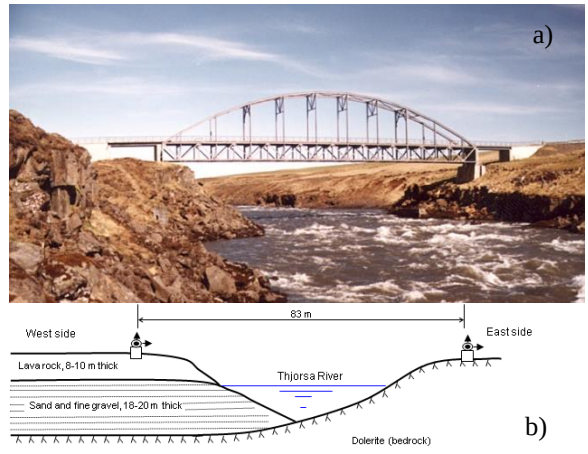

Figure 35. a) The Thjórsá bridge. The left pier is resting on lava rock but the right pier is resting on bedrock. b) schematic cross section of the Thjórsá bridge. Figure courtesy of B. Bessason.

The three recorded acceleration time histories from the west and east abutments during the earthquake are shown in Figure 36.

The observed peak ground acceleration (PGA) was 53% and 120% higher respectively in the N_S versus E_W components on the western abutment compared to the eastern abutment.

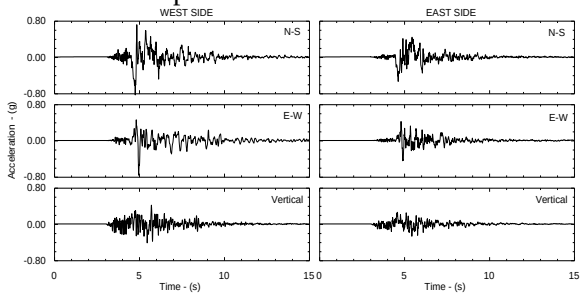

Figure 36. Recorded acceleration time histories at the Thjórsá bridge abutments. Figure courtesy of B. Bessason.

This was further seen clearly in the elastic response spectra of the two sides, as shown in Figure 37 where the sesimic coefficient (horizontal over vertical spectral values) are shown.

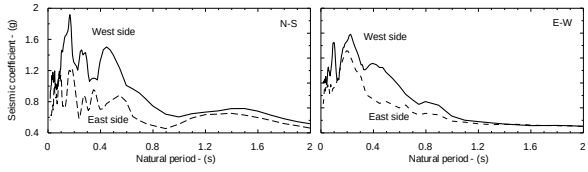

Figure 37. Elastic response spectra (ς=5%) on each side of the Thjorsa River canyon for the earthquake occurring on 21 June 2000 (M=6.5, PGA=0.84g). Figure courtesy of B. Bessason.

The complex lava strata of the western side show some considerable amplification compared to the simpler eastern side where the abutment rests directly on bedrock. The western side fits poorly in the soil categories defined in Eurocode 8.

5.4 Road structures

Large parts of the Icelandic road network consist of thin flexible pavements with either a Hot Mix Asphalt layer or Bituminous Surface Treatments as the surface course over unbound base course and subbase layers. These structures are highly dependent on the performance of the unbound layers. Two typical structures were tested in a full scale Accelerated Pavement Testing (APT) using a Heavy Vehicle Simulator (HVS) testing facility for improving our understanding of the behaviour and the degradation of the structures under heavy loading. In the test over 500,000 rolling wheel load repetitions were applied (Erlingsson & Ingason 2004; Erlingsson 2005 and 2007). The structures were instrumented with deformation sensors, strain gauges and soil pressure cells. A cross section of one of the tested structures is shown in Figure 38.

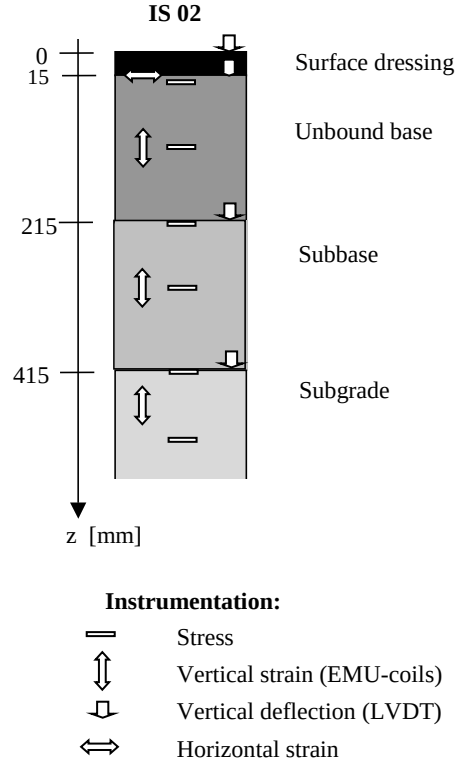

Figure 38. A thin pavement structure tested in an HVS testing facility.

The heavy traffic loading imposes a significant loading in the unbound base and subbase layers of such thin pavement structures. The nonlinear stiffness characterization of these layers is therefore of importance (see Figure 39), where both linear stiffness and non-linear stress dependent stiffness have been used. The stress dependent stiffness M_R has been assumed to follow

$$M_R = k_1 \left(\frac{3p}{p_a} \right)^{k_2} \quad (12)$$

where p is the mean principal stress level, p_a is a reference stress (100 kPa) and k_1 and k_2 are material parameters.

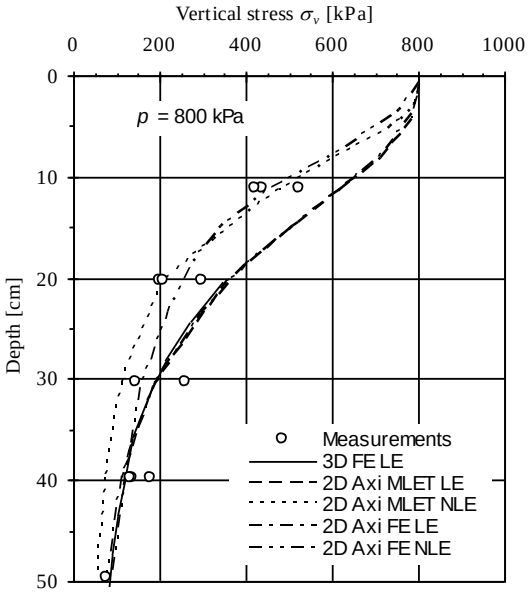

Figure 39. Induced vertical stress under the centre of a single tyre as a function of depth. The axle load was 120 kN and the tyre pressure 800 kPa. 3D = three dimensional analysis, 2D Axi = two dimensional axisymmetric analysis, MLT = Multilayer theory, FE = finite element, LE = linear elastic, NLE non-linenar stress dependent elastic.

Rutting predictions were then carried out using a simple power law function that gave a good agreement with actual measurements of permanent deformation development (see Figure 40).

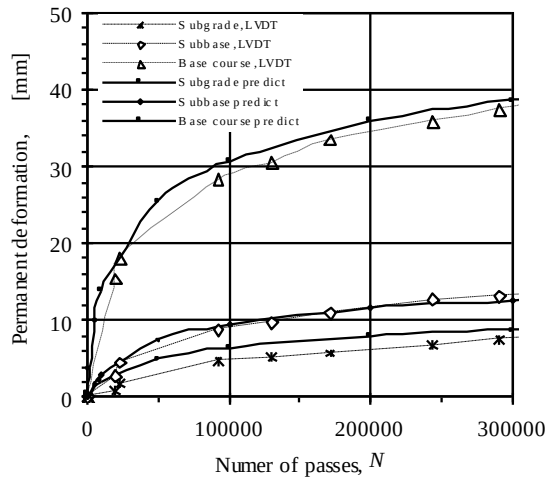

Figure 40. Rutting prediction versus measurements of permanent deformation development as a function of load repetition. The permanent deformation development of each layer is shown (subgrade, subbase, base course) as well as their sum (top line) which is manifested on the surface as rutting. LVDT= Linear Variable Deflectometer Transducers at the top of each layer, predict = prediction based on the numerical anlyses.

A new pavement design method and performance prediction scheme has been developed based on this. For further details, see Erlingsson and Ahmed (2013 and 2019) and Saevarsdottir and Erlingsson (2015).

6 NEW CHALLENGES

The effects of climate changes have created new geotechnical challenges. Two of them are related to retreats of the glaciers and sea level risings. They will be mentioned here briefly. Furthermore, ongoing development of a greenhouse gas mitigation method will be described.

6.1 Glacial retreats

Glaciers cover about 11% of the country (Björnsson and Pálsson, 2008; Hannesdóttir et al. 2014). Since 1995, the glacier mass loss due to climate warming has been continuous, and between 1995 and 2010 the largest ice cap, the Vatnajökull Glacier, lost almost 4% of its volume (Björnsson et al., 2013). This has caused significant changes on and around the present-day outlet glaciers.

The rapidly retreating outlet glaciers often leave steep valley sides behind which may become unstable because of loss of buttressing by the glacier, permafrost degradation and other factors (Stoffel, 2012).

One example of such mass movements has taken place at Svínafellsheiði due to the retreat of the Svínafellsjökull (part of the Vatnajökull Glacier). In 2014, over a100 m long and up to 30 cm wide fracture in bedrock was discovered in the Svínafellsheiði mountain slope. The fracture is located at 850 m a.s.l. in the uppermost part of a 500 m high, almost vertical mountainside (Sæmundsson et al. 2019).

Figure 41. The Svínafellsheiði mountain slope. The solid black line marks the boundary between the topmost basalt layer and underlying móberg/hyaloclastite, the dotted black line shows the observed fracture, and the transparent red polygons shows the overhangs in the basaltic area. Figure courtesy of Þ. Sæmundsson.

6.2 Sea level rising

Due to the complex geological activity and tectonic movements of the country as well as the retreat of the large icecaps, irregular vertical displacement continues to take place on the Iceland plateau. Figure 42 shows the uplift measurements in Iceland during the period 2004 – 2016. On average the land rise is about 1 cm per year, but with high spatial variations (Valsson 2019). These vertical movements affect the design of sea portals and other near- coast structures. In the south-east the uplift is about 3.5 cm/year and probably to a large extent due to the large mass reduction of the Vatnajökull icecap. In other areas hardly any uplift has been measured or even sinking movements observed. For the capital area an average sinking movement of 0.6 mm/y has been observed during these 12 years. For the period 1993 – 2004 the sinking movements were about 2 mm per year.

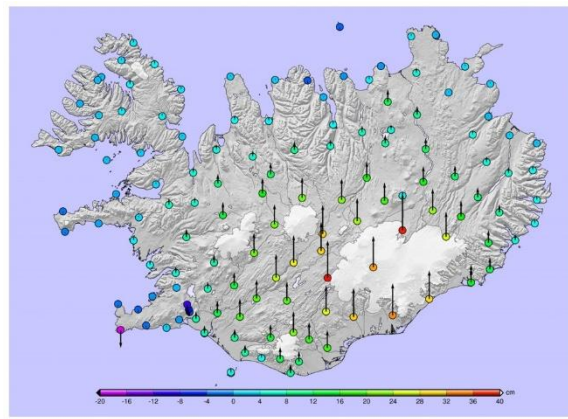

Figure 42. Vertical movements during the period 2004 – 2016 observed by GPS measurements. Figure courtesy of G. Valsson.

6.3 Turning gas into rock by fixation

Five major geothermal plants (> 50 MW) exist in Iceland, of which the Hellisheiði Power station is the biggest (303 MW). Like all other geothermal power plants, the Hellisheiði power plant emits geothermal gases such as the greenhouse gas carbon dioxide (CO_2), but also hydrogen sulfide (H_2S). The CO_2 emission is, however, only a fraction of that stemming from fossil-fuel generation. A new method has been under

development to mineralize the carbon- dioxide and hydrogen-sulphide by turning gas into rock, referred to as mineralization (www.carbfix.com). The CO_2-H_2S gases emitted from the power plant are captured into condensate water from the power plant in a scrubber and the gas-charged water injected deep into the hot basaltic rocks (>700m and >250°C) close to the power plant (Gunnarsson et al. 2018). Basalt plays an important role in this mineralization process as it contains a high amount of calcium, magnesium and iron which interact with the CO_2 and H_2S to form minerals like calcite ($CaCO_2$) and pyrite (fool's gold; FeS_2) (see Figure 43). The mineralization has proven to take less than a year at elevated temperatures and less than two years at 20-50°C, and the minerals can be stable for over centuries or even millions of years (Gislason and Oelkers 2014, Matter et al. 2016). The method can be utilized wherever carbon-dioxide is emitted in the vicinity of basaltic rock and close to water or sea-water sources.

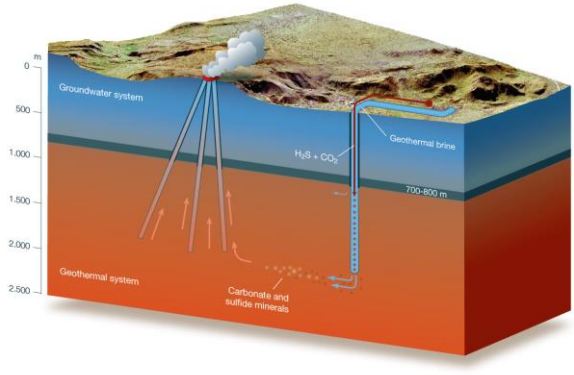

Figure 43. Schematic cross section of the CarbFix2 injection site. Gas-charged and effluent water are injected separately to a depth of 750 m and then allowed to mix until they enter the aquifer at a depth of 1900–2200 m. This combined fluid flows down a hydraulic pressure gradient to monitoring wells. Figure courtesy of S. R. Gislason.

7 CONCLUSION

During the last 100 years, the Icelandic society has gone through extreme changes from being one of the poorest in Europe to a wealthy country with well functioning infrastructure. Geotechnology and related fields have played an important role in this transition related to construction and maintenance of portals, roads, bridges and tunnels, and harvesting of the hydropower as well as of geothermal energy. This paper has given a short overview of the geotechnical conditions in the country. Furthermore, some geotechnical engineering projects have been described. Finally, some new geotechnical challenges due to climate changes have been briefly introduced.

8 ACKNOWLEDGEMENT

B. Bessason (University of Iceland), H. Bjarnason (National Power Company), S. R. Gíslason (University of Iceland), G. V. Guðmundsson (Icelandic Road and Coastal Administration), B.A. Harðarson (Geotek), E. H. Hjálmarsson (IAV), Á. Höskuldsson (University of Iceland), V.A. Ingólfsson, (Icelandic Road and Coastal Administration), B. Jónsson (University of Iceland), H. Sigursteinsson (Icelandic Road and Coastal Administration), J. Sólnes (University of Iceland);, G. Valsson (National Land Survey of Iceland), Þ. Þorsteinsson (University of Iceland).

9 REFERENCES

Árnadóttir, Th., Lund B., Jiang, W., Geirsson, H., Björnsson, H., Einarsson, P., Sigurdsson T. 2009. Glacial rebound and plate spreading: Results from the first countrywide GPS observations in Iceland. *Geophys. J. Int.*, 177(2), 691-716, doi: 10.1111/j.1365-246X.2008.04059.x.

Baldi, G., Bellotti, R., Ghionna, V.N., Jamiolkowski M., LoPresti D.C.F. 1989. Modulus of sands from CPTs and DMTs. *Proceedings of the 12th International Conference on Soil Mechanics and Foundation Engineering*, 13-18 August 1989, Rio de Janeiro, Brazil, Vol. 1, pp. 165-170.

Bessason, B., Kaynia, A.M. (2002). Site amplification in lava rock on soft sediments, *Soil Dynamics and Earthquake Engineering*, 22(7);525-540.

Bjarnason, H., Palmason, P.R, Arnalds, S.S., Adalsteinsson, H. 2019. *Hydropower and Large Dams in Iceland*. Icelandic Committee on Large Dams (ISCOLD), Reykjavik.

Björnsson, H., Pálsson, F. 2008. Icelandic glaciers. *Jökull*, 58, 365–386.

Björnsson, H., Pálsson, F., Guðmundsson, S., Magnússon, E., Aðalgeirsdóttir, G., Jõhannesson, T., Berthier E., Sigurðsson, O., Thorsteinsson T. 2013. Contribution of Icelandic ice caps to sea level rise: Trends and variability since the Little Ice Age. *Geophysical Research Letters*, 40, 1546–1550, doi:10.1002/grl.50278.

Einarsson, P. 2008. Plate boundaries, rifts and transforms in Iceland. *Jökull*, 58, 35-58.

Erlingsson, S. 2005. Numerical modelling of unbound granular materials in thin pavement structures. *Proceedings of the 16th International Conference on Soil Mechanics and Geotechnical Engineering*, Osaka, Japan, 12 – 16 September, pp.1699-1702.

Erlingsson, S. 2007. Numerical modelling of thin pavements behaviour in accelerated HVS tests. *Road Materials and Pavement Design, an International Journal*. Vol. 8/4, pp. 719 - 744.

Erlingsson, S., Ahmed, A. W. 2013. Fast layered elastic response program for the analysis of flexible pavement structures, *Road Materials and Pavement Design*, Vol. 14, No. 1, pp. 196-210. DOI:10.1080/14680629.2012. 757558.

Erlingsson, S., Ahmed, A.W. 2019. Mechanistic rutting modelling of a LTPP road structure. In Crispino, M. (Ed.) *Pavement and Asset Management*. CRC Press/Balkema Taylor, 2019 Taylor & Francis Group, London, UK. ISBN 978-0-367-20989-6, pp. 241-249.

Erlingsson, S., Ingason, Th. 2004. Performance of Two Thin Pavement Structures During Accelerated Pavement Testing Using a Heavy Vehicle Simulator. *Proceedings of the 2nd International Conference on Accelerated Pavement Testing*, Minnesota, 26 – 29 September, 15 pp.

Erlingsson, S., Olafsdottir, E.A., Bessason, B. 2017. Stiffness of sandy sites using the Multichannel Analysis of Surface Waves method. *Proceedings of the 19th International Conference on Soil Mechanics and Geotechnical Engineering,* Seoul, Korea, 17 – 22 Sept. 2017.

Flóvenz, Ó.G. 2019. Geothermal exploitation in Iceland – Success and Challenges. *Proceedings of the 17th European Conference on Soil Mechanics and Geotechnical Engineering*, 1 – 6 September, Reykjavík.

Friðriksson, G. 2013. *Hér heilsast skipin, fyrra bindi* (In Icelandic). Uppheimar.

Gazetas, G. 1991. Foundation Vibrations. *Foundation Engineering Handbook, 2nd edition* (Ed. Fang, H.-Y.), 553–593. Van Nostrand Reinhold, New York, NY.

Gislason S.R., Oelkers, E.H. 2014. Carbon storage in basalt. *Science* 344, 373-374.

Green, R.A., Halldorsson, B., Kurtulus, A., Steinarsson, H., Erlendsson, O.A. 2012. Unique liquefaction case study from the 29 May 2008, M_w6.3 Olfus earthquake, Southwest Iceland. In: *15th World Conference on Earthquake Engineering*, Lisbon, Portugal.

Guðmundsson, Á., Jóhannesson, H., Harðarsson, B.A. 1991. Hvalfjörður Tunnel, Geological report, *Stratigraphy and Structure*. Reykjavík, October, 51 p.

Gunnarsson, I., Aradóttir, E.S., Oelkers, E.H., Clark, D.E., Arnarson, M.Þ., Sigfússon, B., Snæbjörnsdóttir, S.Ó., Matter, J.M., Stute M., Júlíusson, B.M., Gíslason, S.R. 2018. The rapid and cost-effective capture and

subsurface mineral storage of carbon and sulfur at the CarbFix2 site. *International Journal of Greenhouse Gas Control* 79, 117-126.

Hannesdóttir, H., Björnsson, H., Pálsson, F., Aðalgeirsdóttir, G., Guðmundsson, S. 2014. Area, volume and mass changes of southeast Vatnajökull ice cap, Iceland, from the Little Ice Age maximum in the late 19th century to 2010. *The Cryosphere Discuss*., 8, 4681–4735.

Hegazy, Y.A., Mayne, P.W. 1995. Statistical correlations between V_S and cone penetration data for different soil types. *Proceedings of the International Symposium on Cone Penetration Testing, CPT '95*, 4-5 October 1995, Linköping, Sweden, Vol. 2, pp. 173-178.

Hemmingsen, P.K. 2016. *Spennur í íslensku bergi – samantekt á bergspennumælingum á Íslandi* (In Icelandic). MS thesis. Faculty of Civil and Environmental Engineering, University of Iceland.

Hudson, J., Harrison, J. 2002. *Engineering Rock Mechanics: An Introduction to the Principles*. Oxford.

Janbu, N. 1970. *Grunnlag i Geoteknikk* (In Norwegian). Tapir Forlag. Trondheim.

Jóhannsson, Æ. 1997. *Mechanical Properties of Rock in Icelandic Lava Stratum*. M.Sc. thesis. Dept. of Civil and Environmental Engineering University of Iceland.

Kramer, S.L. 1996. *Geotechnical Earthquake Engineering*, Prentice-Hall, Inc., Upper Saddle River, NJ.

Loftsson, M., Ingimarsson, A.K., Jóhannesson, Æ. 2006. In situ rock mass stresses in Iceland and rock mass deformation of underground caverns in the Kárahnjúkar and Blanda Hydroelectric Projects. *ISRM In Situ Rock Stress Conference*, June 2006.

Loftsson, M., Jóhannesson, Æ., Erlingsson, E. 2005. Kárahnjúkar Hydroelectric Project – Powerhouse Cavern. Successful excavation despite complex geology and stress induced stability problems: *26.1-26.25, Proceedings Fjellsprengningskonferansen*, Oslo, 24-25 November 2005.

Matter, J.M., Stute M., Snæbjörnsdóttir, S.Ó., Oelkers, E.H., Gíslason, S.R., Aradóttir, E.S., Sigfusson, B., Gunnarsson, I., Sigurdardóttir H., Gunnlaugsson, E., Axelsson, G., Alfredsson, H.A., Wolff-Boenisch, D., Mesfin, K., Fernandez de la Reguera Taya, D., Hall, J., Dideriksen K., Broecker, W.S. 2016. Rapid carbon mineralization for permanent disposal of anthropogenic carbon dioxide emissions. *Science* 352, 1312-1314.

Mayne, P.W. 2007. *Cone Penetration Testing State-of-Practice*. NCHRP Project 20-05, Topic 37-14, Synthesis 368 on Cone Penetration Testing, February 2007.

NGI. 2015. *Using the Q-system, Rock Mass Classification and Support Design*. NGI, Oslo.

Ólafsdóttir, E.Á., Bessason, B., Erlingsson, S. 2019a. Stiffness profiles of earth dams based on the MASW technique. *Proceedings of the XVII European Conference on Soil Mechanics and Geotechnical Engineering*, Reykjavík, Iceland.

Ólafsdottir, E.Á., Bessason, B., Erlingsson, S. 2019b. Application of MASW in the South Iceland Seismic Zone. Chapter 5 in: Rupakhety R., Olafsson, S. and Bessason B. (eds.) *Proceedings of the International conference on Earthquake Engineering and Structural Dynamics*, Springer, pp. 53 – 66.

Ólafsdóttir, E.Á., Erlingsson, S., Bessason, B. 2018. Tool for analysis of multichannel analysis of surface waves (MASW) field data and evaluation of shear wave velocity profiles of soil, *Canadian Geotechnical Journal* **55**(2), 217-233.

Pálmason, P.R. 2018. *Embankment dam design in Iceland – conceptual considerations*. Landsvirkjun, National Poweer Company of Iceland, Report no.: LV-2018-091. 27 pp.

Park, C.B., Miller, R.D., Xia, J. 1999. Multichannel analysis of surface waves. *Geophysics, 64*(3), 800–808. doi:10.1190/ 1.1444590.

Piratheepan, P. 2002. *Estimating Shear-Wave Velocity from SPT and CPT Data*. (Master of Science Thesis). Clemson University, Clemson, SC.

Robertson, P.K. 1990. Soil classification using the cone penetration test. *Canadian Geotechnical Journal 27* (1), 151-158.

Robertson, P.K. 2009. Interpretation of cone penetration tests - unified approach. *Canadian Geotechnical Journal* 46 (11), 1337-1355.

Saevarsdottir, Th., Erlingsson, S. 2015. Modelling of responses and rutting profile of a flexible pavement structure in an HVS. *Road Materials and Pavement Design*. Vol. 16/1, pp 1-18. DOI: 10.1080/14680629.2014. 939698.

Sæmundsson, Þ., Helgason, J.K., Ben-Yehoshua, D., Bergsson, B. H., Ófeigsson, B., Magnússon, E., Hjartardóttir, Á.R., Drouin, V., Belart, J.M-C., Grímsdóttir, H., Pedersen, G.B.M., Pálsson, F., Guðmundsson, S., Geirsson, H. 2019. Risk of major rock slope failure at the Svínafellsheiði mountain, SE Iceland. *Geophysical Research Abstracts*, Vol. 21, EGU2019-9650, EGU General Assembly.

Sheory, P.R. 1994. A theory for in situ stresses in isotropic and transversely isotropic rock. *Int. J. Rock Mech. Min. Sci. & Geomech. Abstr*. **31**(1), 23-34.

Sigbjörnsson, R., Snæbjörnsson,·J.Th., Higgins, S.M., Halldórsson, B., Ólafsson, S. 2009. A note on the Mw 6.3 earthquake in Iceland on 29 May 2008 at 15:45 UTC. *Bulletin of Earthquake Engineering, 7,* 113–126. doi:10.1007/s10518-008-9087-0.

Skúlason, J. 1978. *Rannsóknir á sigeiginleikum efna ákvörðuðum í ödometer* (in Icelandic). Vegagerð ríkisins, 26 pp.

Skúlason, J., Júlíusson, E., Þórðarson, O. Hilmarsson, H. 2002. *Eiginleikar íslenskra jarðefna gagnvart sveifluálagi* (In Icelandic). Rannsóknastofnun Byggingariðnaðarins. Reykjavík.

Sólnes, J., Sigmundsson, F., Bessason, B. (Eds) 2013. *Náttúruvá á Íslandi Eldgos og jarðskjálftar*, University of Iceland Press and Natural Catastrophe Insurance of Iceland (in Icelandic).

Stoffel, M., Huggel, C. 2012. Effects of climate change on mass movements in mountain environments. *Progress in physical geography*, 36(3), 421–439.

Sykora, D.W., Stokoe, K.H. 1983. *Correlations of In Situ Measurements in Sands With Shear Wave Velocity. Geotechnical Engineering Report GR83-33*. The University of Texas, Austin, TX.

Thordarson, T., Höskuldsson, Á., 2014. Iceland. Dunedin Academic Press, 2nd edition. *Classic Geology in Europe series*, 192 pp. ISBN: 978-1-780-46-021-5.

Þórðarson, S. 2002. *Frumherjar í verkfræði á Íslandi* (In Icelandic). Verkfræðingafélag Íslands.

Tsuchida, H. 1970. Prediction and countermeasure against the liquefaction in sand deposits. In: *Abstract of the Seminar in the Port and Harbor Research Institute*, Yokohama, Japan, pp. 3.1-3.33

Valsson, G. 2019. *Endurmæling ISNET 2016 grunnstöðvanetsins og nýjar viðmiðanir fyrir landmælingar og kortagerð á Íslandi* (In Icelandic). Akranes: Landmælingar Íslands.

Wells, H. 2009. *Liquefaction Potential at a Proposed Hydroelectric Site in Iceland: Urridafoss Case Study Using Cone Penetration Data*. MS thesis, Faculty of Civil and Environmental Engineering University of Iceland, 119 pp.